To do: Delete a note to myself at the end of the caption for Fig.2.12.3.

2.12 Outflow Plumes

One of the most important aspects of deep ocean overflows is the mixing and water mass modification that occurs as dense water spills over a sill and descends down the continental slope. These flows undergo turbulent mixing and entrainment leading to significant dilution and to increases in volume flux by 200% or more. The mixing may be due to bottom boundary layer turbulence or to interfacial instability or both. Bottom and interfacial drag may also be particularly important in determining the path that the flow takes. The portion of the overflow in which these processes are active normally extends from the sill to some point tens or hundreds of kilometers downstream and is called the *plume* or *outflow plume.* It is a sub-region of the *overflow*, meaning the entire hydraulically-driven flow that begins at the upstream mouth of the channel and ends at the downstream extent of the plume.

(a) Frictional plumes in a channel.

Some insights into the structure of a plume can be gained by comparing sections taken downstream of the Faroe-Bank Channel flow (2.11.4-2.11.6) showing the lateral spreading and thinning of the flow in the downstream direction. As the plume descends it becomes thinner and wider and is increasingly confined to the right-hand slope of the channel. These features have been reproduced in a laboratory model (Davies et al 2006) with a V-shaped channel that approximates the Faroe-Bank Channel bathymetry downstream of the sill (Figure 2.12.1). The observer faces upstream and the upper and lower frames show upstream and downstream sections of a particular realization of the plume. Variations in greyscale correspond to variations in density. Three main water masses can be distinguished and these consist of a quiescent overlying fluid (middle grey), a dense core region (dark) lying within the plume, and an intermediate interfacial region (light grey) consisting of mixed fluid. Comparison of the upstream and downstream sections shows that the thickest portion of the core region has shifted from the bottom of the V-shaped channel to higher up on the slope, possibly indicating lateral motion from right to left in the figure. The lateral spreading and thinning of the plume in the downstream section is also evident.

It is difficult to configure laboratory experiments to match all the relevant nondimensional scale ratios that characterize the ocean application. In the above experiment it is possible to match quantities like the average Froude and Rossby numbers $V/(g'D)^{1/2}$ and V/fW, where V, D, and L are velocity, depth and width scales for the plume). More difficult to match is the Reynolds number $R_e=VD/\nu$, where ν is the kinematic viscosity of water. The magnitude of R_e potentially determines characteristics of the turbulence that lead to mixing and entrainment. Values for the present experiment lie in the range 1400-1600 whereas ocean values are $O(10^8)$. However the dependence of the flow on R_e considerably weakens when the threshold value of 1500-2000 is exceeded (Davies et al. 2002) and this scenario is approached in the experiment.

Deductive analytical models of plumes are generally not available due to the difficulty in dealing with the combined effects of friction, entrainment and nonlinear advection. However there are some very helpful models that rely partially on ad hoc assumptions. We will discuss two such models. The first ignores entrainment but includes some elementary Ekman layer effects. The second includes both frictional drag and entrainment but does so within the context of a 'streamtube' flow that has uniform properties across each section. The flow takes place on a uniformly tilting plane.

In the Davies et al. 2006 model, the flow is confined to a V-shaped channel that has side slopes α and -α (Figure 2.12.2, viewed from upstream) and that tilts downhill with uniform slope *S*. The flow grounds on the left and right slopes at positions $x^*=x_L^*$ and $x^*=x_R^*$ as shown. The neglect of entrainment allows for a second simplifying assumption, namely that the flow is locally uniform in y^*. Changes in the flow along its path can then occur only as a result of changes in the bottom slopes (α or *S*), which are allowed to vary gradually with y^*. Finally, it is assumed that the plume thickness d^* is much greater than the thickness of bottom or interfacial frictional layers and that the inviscid core region is in geostrophic balance in both directions. Thus the along-channel inertial effects fundamental to hydraulic behavior will be absent.

The geostrophic relations for the two velocity components in the inviscid core are

$$u^* = \frac{g}{f} S \tag{2.12.1}$$

and

$$v^* = \frac{g}{f}\frac{\partial}{\partial x^*}(d^* + h^*) = \frac{g}{f}\frac{\partial d^*}{\partial x^*} + \frac{g}{f}\begin{cases} \alpha & (x>0) \\ -\alpha & (x<0) \end{cases}. \tag{2.12.2}$$

The volume flux associated with the core region is

$$\begin{aligned} Q^* &= \int_{x_L^*}^{x_R^*} v^* d^* (dx^*) = \frac{g}{f}\int_{x_L^*}^{x_R^*} d^* \left(\frac{g}{f}\frac{\partial d^*}{\partial x^*} + \frac{g}{f}\begin{cases} \alpha & (x>0) \\ -\alpha & (x<0) \end{cases} \right) dx^* \\ &= \frac{\alpha g}{f}\left(\int_{x_L^*}^{0} (d^*) dx^* - \int_{0}^{x_R^*} (d^*) dx^* \right) \end{aligned} \tag{2.12.3}$$

in which $d^*(x_L^*) = d^*(x_R^*) = 0$ has been used. The flux in any frictional boundary layers at the top or bottom must be added to Q^* to get the total volume flux, but these contributions are small.

The depth-integrated transport of volume in the x^*-direction consists of a contribution d^*u^* from the core velocity, plus a contribution from the frictional boundary layers. In the present circumstance the latter is an Ekman layer and it characteristics are

discussed in most texts on geophysical fluid dynamics [e.g. Pedlosky (1987), Ch. 4]. For a laminar flow the Ekman layer thickness is $\delta_E = (2\nu / f)^{1/2}$, but ν must be replaced by a hypothetical turbulent viscosity in the context of the experiment or application. If the overlying geostrophic flow is directed primarily in the *y*-direction, which is the case here, then a transport in the negative *x** direction equal to $v^* \delta_E / 2$ takes place in the boundary layer. Davies et al. (2006) assume that a similar frictional layer occurs at the upper interface and thus the total boundary layer transport is $v^* \delta_E$.

Since the flow is independent of *y**, the depth integrated mass flux in the *x**-direction is nondivergent. This flux is clearly zero at the edges of the plume and the flux must therefore be zero everywhere else:

$$u^* d^* - v^* \delta_E = 0 . \qquad (2.12.4)$$

Use of (2.12.1) and (2.12.2) to substitute for the velocities leads to

$$\frac{\partial d^*}{\partial x^*} - \frac{S}{\delta_E} d^* = \begin{cases} \alpha & (x > 0) \\ -\alpha & (x < 0) \end{cases} . \qquad (2.12.5)$$

The solutions in the two regions are given by

$$d^* = \begin{cases} Be^{\phi x^*/\delta_E} + \alpha\delta_E / S & (x > 0) \\ Ae^{\phi x^*/\delta_E} - \alpha\delta_E / S & (x < 0) \end{cases} . \qquad (2.12.6)$$

The solution on each tilting side slope therefore consists of a uniform region with constant layer thickness and an outer boundary layer of width δ_E/S that brings the thickness to zero. The theory formally breaks down as the depth vanishes since there is nothing to balance the Ekman flux in (2.12.4). The fact that the thickness is brought to zero monotonically means the slope of the interface cannot be greater than the slope of the bottom.

Matching the two solutions across *x**=0 leads to

$$A = B + 2\alpha\delta_E / S .$$

In addition the position of the right-hand outcrop is given by setting *d**=0 in the first relation in (2.12.6):

$$B = -\frac{\alpha\delta_E}{S} e^{-Sx_R^*/\delta_E} .$$

The full solution is therefore

$$d^* = \frac{\alpha\delta_E}{S}\begin{cases} 1 - e^{S(x^*-x_R^*)/\delta_E} & (x^* > 0) \\ \left[(2 - e^{-Sx_R^*/\delta_E})e^{Sx^*/\delta_E} - 1\right] & (x^* < 0) \end{cases} \qquad (2.12.7)$$

The position of the left edge of the current can be obtained by setting $d^*=0$ in the second part of (2.12.7):

$$(2 - e^{-Sx_R^*/\delta_E})e^{Sx_L^*/\delta_E} = 1\,. \qquad (2.12.8)$$

The flux Q is computed from (2.12.3) as

$$Q = \frac{\alpha^2 g\delta_E^{\,2}}{fS^2}\left[\frac{S}{\delta_E}(x_R^* - x_L^*) + 2(e^{-Sx_R^*/\delta_E} - 1)\right], \qquad (2.12.9)$$

and edge positions x_R^* and x^*_L are related by (2.12.8), or

$$x_L^* = -\frac{\delta_E}{S}\ln(2 - e^{-Sx_R^*/\delta_E})\,. \qquad (2.12.10)$$

As the along-channel slope S decreases the right-hand side of (2.12.9) increases. A constant value of Q can be maintained by increasing the value of x_R^* and thus the right hand edge of the current must broaden as the along-channel slope decreases. This tendency can be understood as follows: When S decreases (and α remains fixed), u decreases while v, and therefore the cross-channel Ekman layer flux remains the same. The layer thickness d must therefore increase to maintain zero net volume transport across the channel. The plume must therefore narrow in order to maintain the same value of Q. We leave it as an exercise for the reader to argue that the opposite effect occurs when α decreases and S is kept constant.

Equation (2.12.9) suggests $\frac{\alpha^2 g\delta_E^{\,2}}{fS^2}$ as a natural scale for Q. A plot of the corresponding nondimensional transport vs. a nondimensional version of x_R^* (Figure 2.12.3) shows that the right side of the plume broadens as the transport increases. This tendency is consistent with what is observed in the experiment (symbols), and to some extent the Faroe Bank Channel overflow.

(b) Streamtube models for entraining plumes.

The previous model is restricted in that it requires a channel geometry and does not allow for entrainment. All major outflow plumes undergo entrainment, though it may only be significant over certain reaches. The plumes associated with outflows from the Mediteranean, the Denmark Strait, and the Weddell Sea's Filchner Ice Shelf ride along continental slopes and gradually descend. A traditional tools for simulating the combined

effects of entrainment and bottom friction in these flows is the streamtube model, pioneered by Smith (1975) and improved by Killworth (1977) and Price and Baringer (1994). We will discuss the original version of this model and comment on later refinements.

The term 'streamtube' implies a coherent flow that can be characterized at any cross section by a few variables that define the bulk properties like average velocity. In the case of the Smith (1975) model the flow takes place on a flat surface with uniform slope S in the y-direction (Figure 2.12.4). Natural coordinates (s^*,n^*) are used to measure distance along and normal to the axis of the plume. The plume properties are assumed to vary gradually in the s^*-direction. Different versions of the model make different assumptions with regard to the variables used to characterize the flow and the way in which entrainment, friction and stratification are handled, but there is one far-reaching assumption make by all. The plume is supposed to be sufficiently thin that the slope of the interface remains nearly equal to the slope of the bottom in any direction. Accordingly, the pressure gradient in the plume is assumed proportional to the bottom slope; contributions from the gradient of the plume depth are neglected. The main consequence of this simplification will be elimination of gravity wave dynamics from the model and thus the transmission of information upstream. As we will see, the steady plume equations can be integrated downstream beginning at some point where the flow properties are known without regard for conditions far downstream. This considerably simplifies the computational problem for ocean applications. However, the local Froude numbers in deep plumes are observed to consistently fall below unity, particularly far downstream of the source, suggesting that upstream wave propagation is possible. The importance of the consequences is not fully understood at the time of this writing.

The plume axis makes an angle β with respect to the x-axis and thus the position (X^*,Y^*) of the plume in the Cartesian frame is given by

$$\frac{dX^*}{ds^*} = \cos\beta \quad \text{and} \quad \frac{dY^*}{ds^*} = \sin\beta\,.$$

The along- and cross- axis velocities will be denoted V^* and U^* respectively, with $|U^*| << |V^*|$ and it will be assumed that V^* and the plume density ρ are constant across the section of the plume at any particular s^*. The overlying fluid is stably stratified and has density $\rho_a(z)$, which can alternatively be expressed as a function of s^* for a given plume path.

Entrainment into the plume is represented as in Section 1.11 by a cross-interface, positive downwards, vertical velocity w_e^*. If A^* is the cross-sectional area of the plume, the volume flux A^*V^* must therefore obey

$$\frac{\partial}{\partial s^*}(A^*V^*) = \int_{n_R^*}^{n_L^*} w_e^*\, dn^*, \qquad (2.12.11)$$

while the total mass flux $\rho A^* V^*$ is subject to

$$\frac{\partial}{\partial s^*}(\rho A^* V^*) = \int_{n_R^*}^{n_L^*} \rho_a w_e^* \, dn^* \cong \rho_a \int_{n_R^*}^{n_L^*} w_e^* \, dn^* . \qquad (2.12.13)$$

Here n_R^* and n_L^* denote the grounding positions of the interface on the right and left edges of the plume, facing downstream.

The along-axis momentum balance for the plume is expressed in terms of the depth-integrated versions of the shallow-water equations, which appear at the beginning of Section 2.1 in Cartesian form. If at a particular section of the plume, the coordinates are aligned such that the former y^* axis coincides with the present s^*-direction, and the former x^* points in the $-n^*$ direction, then the along-axis momentum equation is

$$\frac{\partial}{\partial s^*}\left[\rho_o V^{*2} d^* + \tfrac{1}{2}(\rho - \rho_a) g d^{*2}\right] + \frac{\partial}{\partial n^*}(\rho_o U^* V^* d^*) - f U^* d^* = (\rho - \rho_a) g S \sin\beta - (\tau_B + \tau_I) \qquad (2.12.14)$$

This result may be compared with the depth-integrated momentum equation (1.9.10) for a one-dimensional flow subject to entrainment from above. Note that there is no source of momentum from the entrainment since the overlying fluid is assumed to be motionless (v_1=0 in 1.9.10). There are sinks of momentum from the frictional stresses at the bottom and interface, as represented by τ_B and τ_I. The Boussinesq approximation has been made, meaning that ρ is replaced by a constant reference density ρ_o where it multiplies inertial terms. It will be convenient to choose ρ_o as the density of the plume at some source point where the outflow originates.

Following the assumption that the plume is so thin that the pressure gradient is due entirely to the bottom slope, the term proportional to d^{*2} is neglected. An important consequence is that horizontal pressure gradients due to horizontal variations of density along the path of the plume are ignored. The remaining pressure gradient (first term on the right-hand side) is proportional to the along-axis component of the bottom slope $S\cos\beta$. In addition fU^*d^* is neglected on the basis that U^* is rendered small by the use of the natural coordinate system and the assumption of gradual variations in s^*. This last assumption is not consistent with the usual semi-geostrophic approximation, where in spite of gradual variations the term fU^* must be retained. This and other non-deductive assumptions place the streamtube theory in the realm of *ad hoc* models.

Integration of the simplified version of (2.12.14) across the plume and use of $d^*(n_R^*) = d^*(n_L^*) = 0$ leads to

$$\frac{\partial}{\partial s*}\left(A*V*^2\right) = g'SA*\sin\beta - \int_{x_R*}^{x_L*}[(\tau_B+\tau_I)/\rho_o]dn\,, \qquad (2.12.15)$$

where $A* = \int_{x_R*}^{x_L*}(d*)dn$ and $g' = g(\rho-\rho_a)/\rho_o$.

The cross-stream momentum equation is a form of the geostrophic relation, modified to include the effects curvature along the *s**-axis. The equation is identical to the *n** momentum equation written in a cylindrical coordinate system with *n** as the radial variable (see Batchelor, 1967, Appendix 2) and with the advective terms ignored. (A similar problem will be considered in detail in Section 4.5.) The resulting momentum balance is

$$V*\left(f + V*\frac{d\beta}{ds*}\right) = sg'\cos\beta\,. \qquad (2.12.16)$$

The factor $d\beta/ds*$ is the curvature of the plume axis and $V*d\beta/ds*$ can be thought of as an augmentation of the Coriolis acceleration.

A simple example that provides a reference for further analysis is a non-entraining, frictionless outflow that moves along isobaths (β=0). Equation (2.12.16) gives the velocity of such a flow as

$$V* = \frac{Sg'}{f}\ . \qquad (2.12.17)$$

This formula applies in more general settings as well. It can be shown (Exercise 3) that the right hand side is the average velocity of a geostrophic current flowing along a constant slope, provided the interface elevation is properly taken into account in the calculation of the pressure. The same factor was also shown by Nof (1983) to be the speed of a geostrophically-balanced, lens-like eddy propagating along a slope.

More generally, let g_o' denote the value of reduced gravity at the source. Then the above result suggests Sg_o'/f as a scale for V* and it is natural to then choose $L=Sg_o'/f^2$ as a horizontal length scale. We also scale A* with its upstream value A_o*. The corresponding dimensionless forms of (2.12.11-16) are

$$\frac{\partial}{\partial s}(AV) = E_n\,, \qquad (2.12.17)$$

$$\frac{\partial}{\partial s}\left(\frac{\rho}{\rho_o}AV\right)=\frac{\rho_a}{\rho_o}E_n, \qquad (2.12.18)$$

$$\frac{\partial}{\partial s}\left(AV^2\right)=\gamma A\sin\beta-F_\tau, \qquad (2.12.19)$$

and

$$V\frac{d\beta}{ds}=\gamma\cos\beta-V, \qquad (2.12.20)$$

where $\gamma(s)=(\rho-\rho_a)/(\rho_o-\rho_{ao})$ and ρ_{ao} is the upstream value of ρ_a.

The expressions for entrainment and drag

$$E_n=\frac{1}{fA_o}\int_{n_R^*}^{n_L^*} w_e^*\,dn^* \qquad (2.12.21)$$

and

$$F_\tau=\frac{1}{A_o g_o's}\int_{x_R^*}^{x_L^*}[(\tau_B+\tau_I)/\rho_o]dn \qquad (2.12.22)$$

must be parameterized. The bottom and interfacial stresses are most commonly specified using a quadratic drag law of the form

$$F_\tau=\kappa V^2. \qquad (2.12.23)$$

Entrainment is normally parameterized as described in Section 1.9 in terms of a Froude number. Many of the laboratory experiments or field studies that have been used to develop empirical formulas involve nonrotating flows in which the local Froude number $v/(g'd)^{1/2}$ is constant across the descending stream. Some of the corresponding data is shown in Figure 1.10.4. In the present case the value of $v/(g'd)^{1/2}$ varies across the stream and the parameterization is written in terms of a bulk Froude number characterizing the whole cross-section (Price and Barringer, 1995). For present purposes it is adequate to regard E_n as a function of V and A and make no further specification.

A more general case of uniform flow over the sloping bottom arises if entrainment is ignored ($E_n=0,\rho=\rho_o$) and the overlying fluid is homogeneous ($\rho_a=\rho_{ao}$, and therefore $\gamma=1$). If the friction parameterization (2.12.23) is then used, the velocity and

angle of descent are found by setting $\partial / \partial s = 0$ in equations (2.12.19,21) and setting A to its upstream value of unity. Thus

$$\sin\beta = \kappa V^2 \qquad (2.12.24)$$

and

$$\cos\beta = V\,, \qquad (2.12.25)$$

These relations summarize the force balance (Figure 2.12.5) in which gravity attempts to pull the plume down the fall line, frictions tends to retard the flow, and the Coriolis effect tends to accelerate the plume the right of the velocity. Only the frictional and gravitational forces act parallel to the plume axis and velocity must have a down slope component (β>0) in order for the two to balance. If V is eliminated between the above two relations, it follows that

$$\frac{\sin\beta}{\cos^2\beta} = \kappa \qquad (2.12.26)$$

and thus the angle of descent increases as the friction coefficient increases. If perturbed from this parallel state the plume executes stable meanders about it's original path (see Exercise 4).

When entrainment is present, the flow can no longer be uniform in s, making simple solutions harder to come by. However, if the overlying fluid is homogeneous (ρ_a=constant) then the problem can be simplified somewhat. To begin with, subtraction of the product of ρ_a and (1.12.18) from (1.12.19) yields

$$\frac{\partial}{\partial\xi}\left(\frac{\rho-\rho_a}{\rho_o}AV\right) = 0\,, \qquad (2.12.27)$$

showing that the buoyancy flux

$$B = [(\rho-\rho_a)/\rho_o]AV \qquad (2.12.28)$$

is conserved. At its point of origin (s=0) we will assume that the plume flows parallel to the isobaths (β=0), as it would if entrainment and friction were nil. The upstream values of the plume variables at this point are then $A(0)=V(0)=1$, $\beta(0)=0$, $\rho(0)=\rho_o$, and $\rho_a(0)=\rho_{ao}$. Downstream of this point we will consider the evolution of the flow assuming that entrainment and friction are finite but weak ($E_n<<1$ and $\kappa<<1$). The entrainment may vary with V and A, and it is assumed only that it retains the same general nondimensional size as the friction term, i.e. $E_n(V,A) = O(\kappa)$.

Next expand the dependent variables according to

$$A = 1 + \kappa A^{(1)} + \cdots$$

$$V = 1 + \kappa V^{(1)} + \cdots$$

$$\beta = \kappa \beta^{(1)} + \cdots \qquad (2.12.29)$$

$$\rho = \rho_O + \kappa \rho^{(1)} + \cdots$$

Substitution into (2.12.17,19,20 and 27) and retention only of O(κ) terms leads to

$$\frac{d}{ds}\left(A^{(1)} + V^{(1)}\right) = \frac{E_n}{\kappa},$$

$$\frac{d}{ds}\left(A^{(1)} + 2V^{(1)}\right) = \beta^{(1)} - 1,$$

$$\frac{d\beta^{(1)}}{ds} = \tilde{\rho}^{(1)} - V^{(1)},$$

and

$$\tilde{\rho}^{(1)} = -(V^{(1)} + A^{(1)}).$$

where $\tilde{\rho}^{(1)} = \rho^{(1)} / (\rho_o - \rho_{ao})$.

The solutions satisfying the upstream conditions $\beta^{(1)} = V^{(1)} = A^{(1)} = 0$ are

$$\beta^{(1)} = 1 - \cos s,$$

$$V^{(1)} = -\sin s - \frac{E_n}{\kappa} s,$$

$$A^{(1)} = \sin s + \frac{2E_n}{\kappa} s,$$

and

$$\tilde{\rho}^{(1)} = -\frac{E_n}{\kappa} s.$$

Thus the combined influence of friction and entrainment causes the plume to turn downslope ($\beta^{(1)}$ becomes positive). The velocity V decreases but the area A increases at

twice the rate, this in order for the volume flux to increase. The plume is diluted ($\tilde{\rho}^{(1)}$ becomes negative) in proportion to the entrainment rate $E_n(1,1)$ but in inverse proportion to the drag coefficient. Along with these trends, the plume undergoes a meandering motion with wave length 2π, dimensionally $2\pi Sg_o'/f^2$, caused when the path overshoots the equilibrium angle $\beta^{(1)}=1$ or $\beta=\kappa$. The linear solution remains valid only for distances of order κ^{-1} downstream of the point of origin; the secular growth associated with the terms proportional to s invalidate the asymptotic expansion further downstream.

Application of streamtube models to specific outflows have resulted in a number of refinements, including variable bottom slope and separate treatments of temperature and salinity. In his simulation of the Weddell Sea plume, which is observed to spill to the bottom of the slope, Killworth (1977) notes that the simulated flow will not reach the bottom without inclusion of the *thermobaric* effect, the increase with depth of the coefficient of thermal expansion. A less subtle process is entrainment, which addressed by the Price and Barringer (1995) model. Since the entrainment velocity is parameterized by the Froude number, an explicit treatment of the plume width and depth, and not just the cross section area, is required. Price and Barringer base their treatment on a spreading law in which the downstream rate of increase of the plume width is proportional to the bottom drag.

One of the most important factors determining the fate of ocean plumes is the density of the overlying water. It is well known that the densest source waters come from the Mediterranean Sea, but the densest product waters come from the high latitude overflows (Weddell Sea, FBC and Denmark Strait). For these applications, the least dense source waters tend to produce the densest product waters (Table 2). This is largely due to the fact that the density of the overlying water is greatest where the product water is greatest.

Table 2.1 Densities (σ_θ) of the average source, product and overlying water for four major outflow plumes. (Data from Price and Baringer, 1995).

Location	source	product	ambient (overlying)
Filchner Ice Shelf (Weddell Sea)	27.93	27.89	27.82
Denmark Strait	28.04	27.92	27.72
Faroe Bank Channel	28.07	27.90	27.56
Mediterranean	28.95	27.70	27.06

Exercises.

1) Show that the theory that leads to (2.12.7) fails to provide a solution for the case in which the plume rides entirely over the positively sloping portion of bottom ($x^*>0$), i.e. a solution for with $x_L^*>0$.

2) For the Davies et al. (2006) model, show that the plume broadens when the cross-channel slope α is decreases but ϕ remains fixed.

3) Show that the velocity defined by (2.12.17) is the average velocity of a geostrophic current flowing along a constant slope if the interface elevation is properly taken into account in the calculation of the pressure.

4) *The meandering of a non-entraining plume.* Consider the Smith (1975) streamtube model for the case in which there is no entrainment and where the overlying density is uniform.

(a) Show that the two momentum equations (2.12.19 and 2.12.20) can be written for this case in the form

$$Q\frac{dV}{ds} = \frac{Q\sin\beta}{V} - \kappa V^2 ,$$

and

$$V\frac{d\beta}{ds} = \cos\beta - V ,$$

where $Q=AV$ is the (now constant) volume flux.

(b) For a given Q, show that the fixed point (i.e. $\partial / \partial s = 0$) solutions, which are just the parallel flows discussed earlier, are given by (2.2.26) and

$$\kappa^2 V^4 Q^{-2} + V^2 - 1 = 0 .$$

(c) By linearizing the momentum equations about this solution, show that small departures from the parallel state consists of meanders of the flow axis and calculate the meander wavelength.

(d) Show that motions not restricted to small amplitude perturbations of the parallel state are described by the relationship

$$\frac{d\beta}{dV} = \frac{Q(\cos\beta - V)}{Q\sin\beta - \kappa V^3} .$$

Sketch some of the corresponding solutions in the (V,β) plane and show that they consist of periodic orbits that surround the fixed point calculated in (b).

Note: I have not solved this problem yet for the linear solutions nor have I sketched the periodic orbits to be sure that they are in fact closed. According the Price and Baringer, the solutions are cycloids.

Figure Captions

2.12.1 Dye images two section of a laboratory plume in a V-shape channel. Different shades of gray correspond to different densities, though there is no calibration. The viewer faces upstream. The lighter fluid is a mix between deeper (dark) and upper (middle gray) fluid. (Based on Figure 3 of Davies, et al. 2006)

2.12.2 Definition sketch for Davies et al. 2006 model.

2.12.3 The dimensionless width $\frac{x_R * \phi}{\delta_E \cos\alpha}$. of the right-hand ($x$>0) portion of the current as a function of dimensionless transport Q/Q_s, where $Q_s = \alpha^2 g \delta_E{}^2 / fS^2$. The curve shows the predicted width based on (2.11.19) The symbols represent data from the Davies et al. (2006) experiment. (Figure 11 of Davies et al. 2006).

Author Note: To get the ordinate, their L_s/L, I use their 4.6 and 4.17, in which their L is my δ_E/ϕ. Also their $\hat{X}_L$ is my x_R*/L. Thus

$$Ls / L = \frac{\hat{X}_L \delta_E / \phi \cos\alpha}{\delta_E / \phi} = \frac{\hat{X}_L}{\cos\alpha} = my \frac{x_R * / L}{\cos\alpha} = \frac{x_R * \phi}{\delta_E \cos\alpha}$$

2.12.4 Definition sketch for streamtube model.

2.12.5 The equilibrium state of a descending, non-entraining plume in a homogeneous environment. The dashed arrows show the normal and tangential components of the gravitational force; these must be balanced by the Coriolis acceleration and the frictional drag vectors.

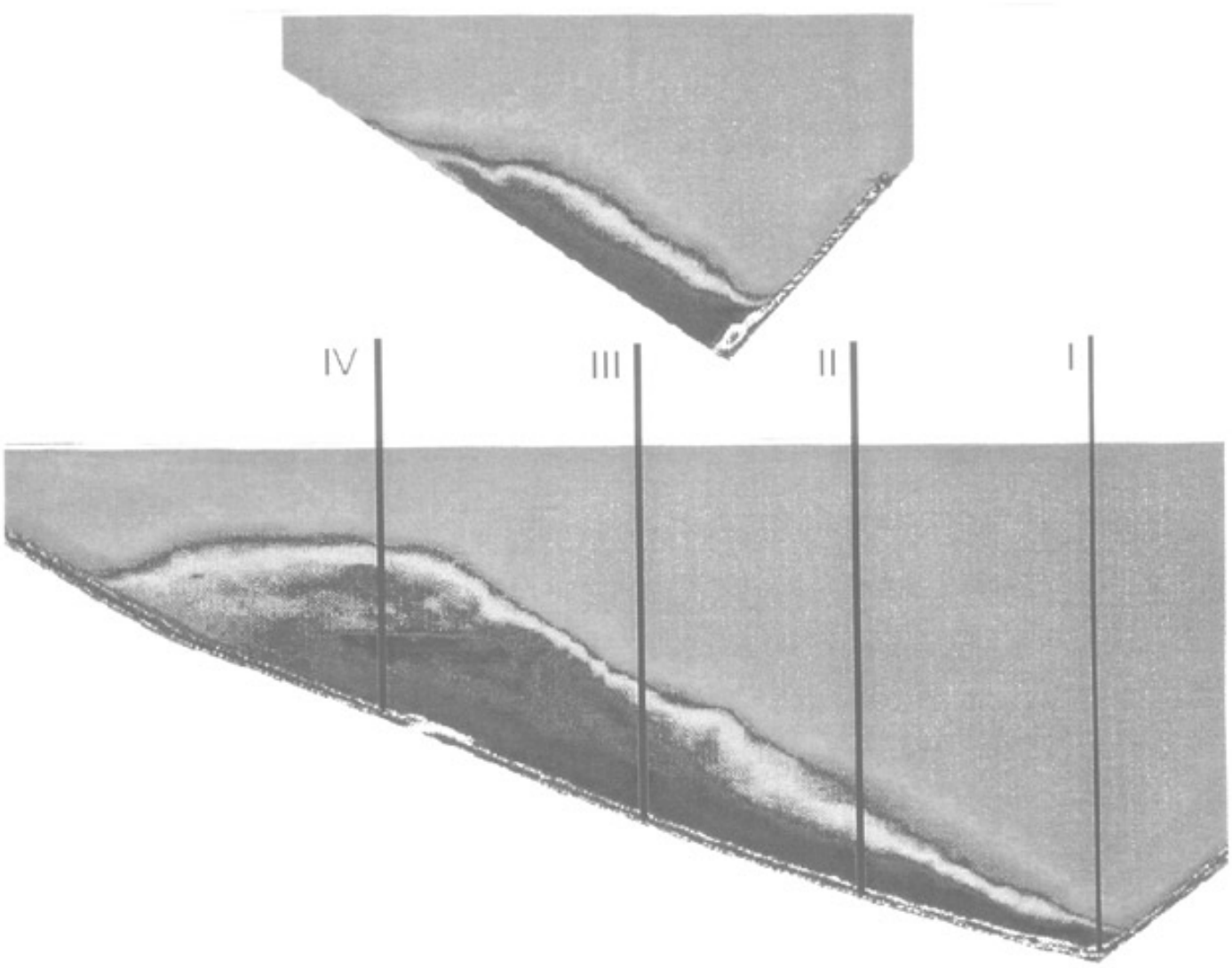

Figure 2.12.1 low resolution, grey scale version

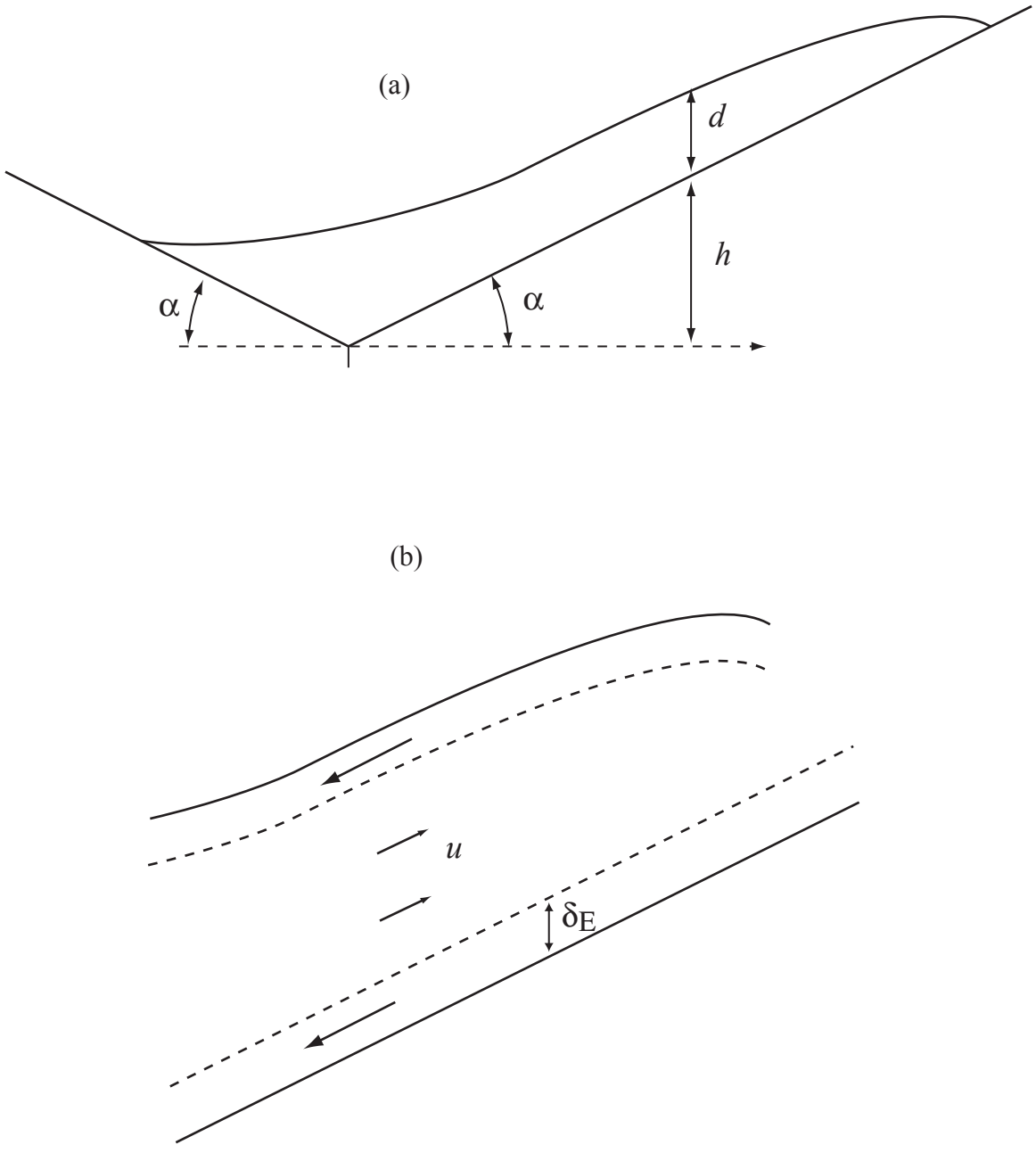

Figure 2.12.2

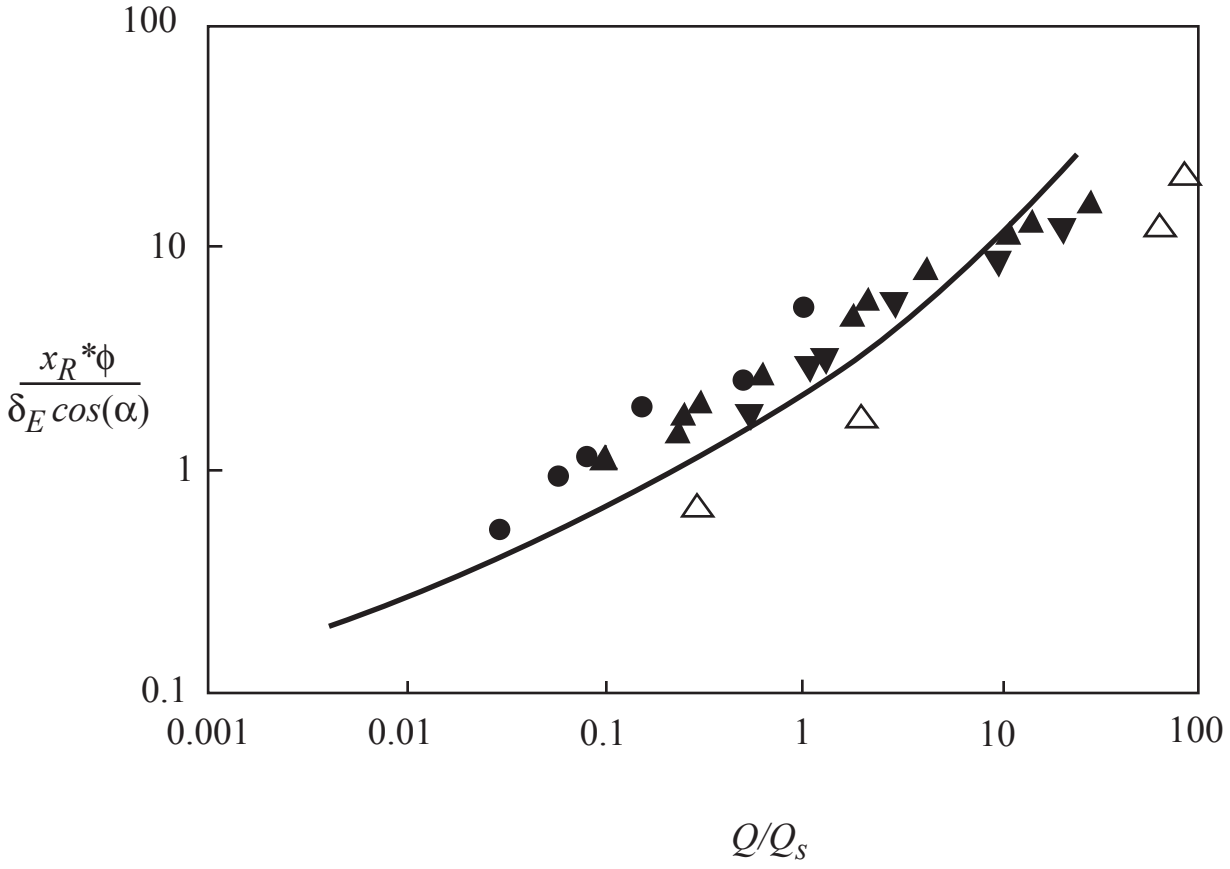

Fig. 2.12.3

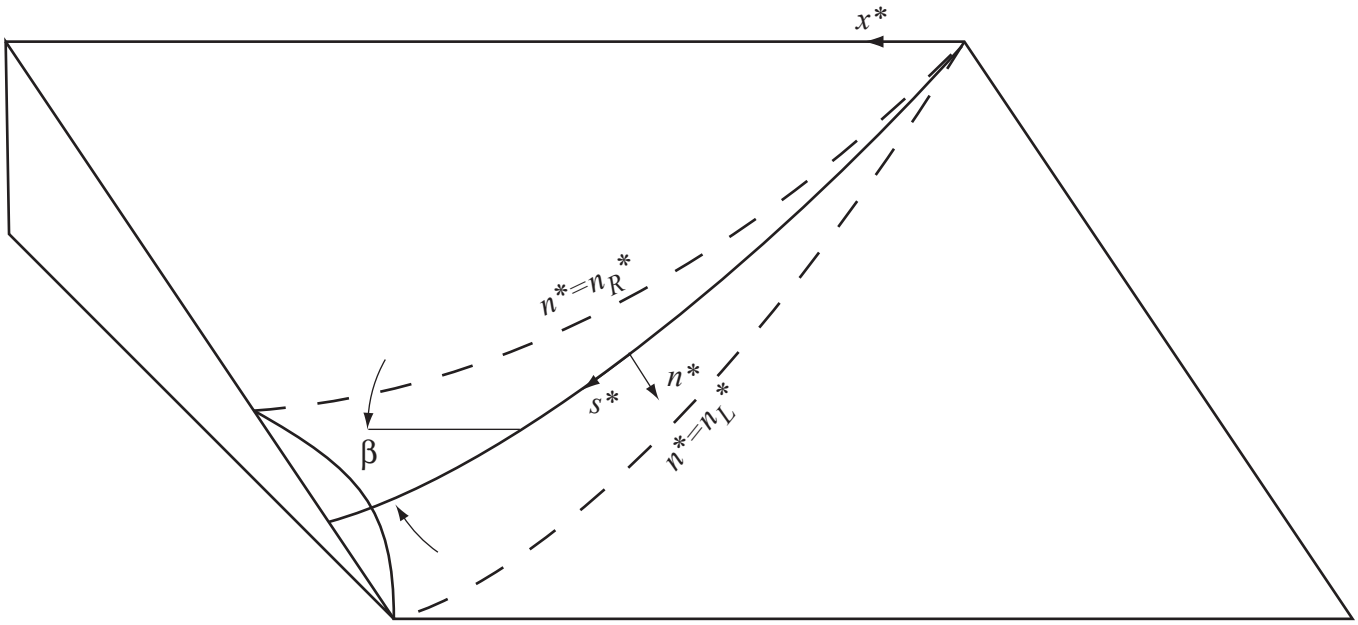

Figure 2.12.4

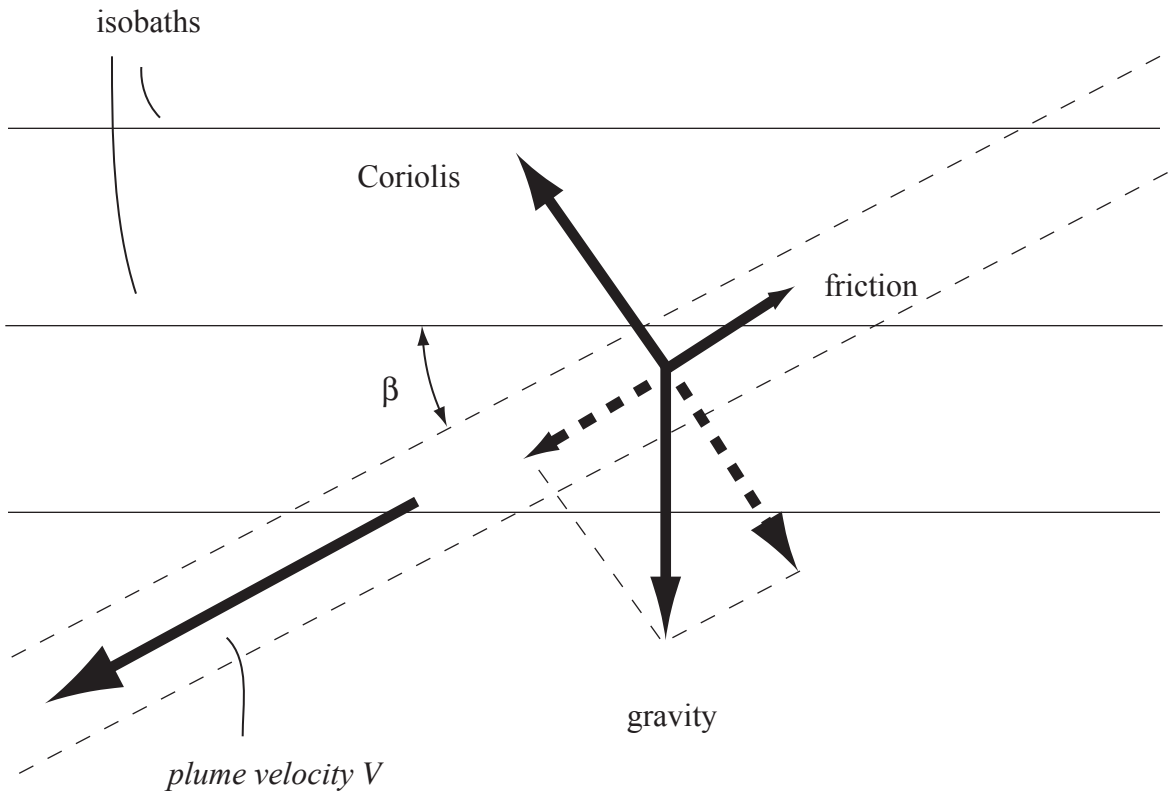

Figure 2.12.5